Accepted Manuscript

Strength hierarchy provisions for transverse confinement systems of shell structural elements

S. Sessa, F. Marmo, N. Vaiana, D. De Gregorio, L. Rosati

PII: S1359-8368(18)32369-2

DOI: https://doi.org/10.1016/j.compositesb.2019.01.018

Reference: JCOMB 6500

To appear in: *Composites Part B*

Received Date: 29 July 2018

Revised Date: 10 October 2018

Accepted Date: 2 January 2019

Please cite this article as: Sessa S, Marmo F, Vaiana N, De Gregorio D, Rosati L, Strength hierarchy provisions for transverse confinement systems of shell structural elements, *Composites Part B* (2019), doi: https://doi.org/10.1016/j.compositesb.2019.01.018.

This is a PDF file of an unedited manuscript that has been accepted for publication. As a service to our customers we are providing this early version of the manuscript. The manuscript will undergo copyediting, typesetting, and review of the resulting proof before it is published in its final form. Please note that during the production process errors may be discovered which could affect the content, and all legal disclaimers that apply to the journal pertain.

ACCEPTED MANUSCRIPT

Strength hierarchy provisions for transverse confinement systems of shell structural elements

S. Sessa[a,*], F. Marmo[a], N. Vaiana[a], D. De Gregorio[a,b], L. Rosati[a,b]

[a] *Department of Structures for Engineering and Architecture, University of Naples Federico II, Via Claudio, 21, 80124, Napoli, Italy*
[b] *PLINIVS Study Centre, via Toledo 402, Naples, Italy*

Abstract

Through-the-thickness (TT) confinement of masonry and concrete panels by composite or steel reinforcements, aiming at seismic retrofit of existing structures, has recently growth in popularity. However, structural design of transversal reinforcements, modeled as an homogeneized material, is often performed by neglecting the cyclic nature of seismic actions and by using static approaches. For this reason, a proper strength hierarchy between the confined core material and the confining devices should be accounted for in order to ensure that the retrofit system remains effective until the crisis of the core material is attained. This research introduces strength hierarchy conditions for TT-confinement systems, made of materials exhibiting a nonlinear behavior, aiming at determining the minimum strength required for uniaxial confining devices. The relevant relationships, theoretically derived by assuming a Drucker Prager constitutive model for the confined material and by enforcing equilibrium and compatibility conditions between the core and the confining devices, are characterized by simple mechanical parameters, usually available in common practice applications, familiar to most of the designers. Numerical examples confirm the effectiveness of the proposed provisions.

Keywords: Through-the-thickness confinement; fiber-reinforced masonry; strength hierarchy.

*Corresponding author
Email address: salvatore.sessa2@unina.it (S. Sessa)

ACCEPTED MANUSCRIPT

1. Introduction

Use of confining devices for retrofitting reinforced concrete (rc) or masonry structures has become a very popular technique because of the well known positive effect induced by confinement on strength and ductility of the core material. In particular, confinement devices introduce a binding effect that enhances the deformative capacity of confined material and induces a transversal stress component able to increase the compressive spherical part of the stress tensor [1, 2, 3]; this last effect, in particular, is highly beneficial for the strength capacity of a large variety of building materials. As a matter of fact, such a strategy turns out to be very efficient for the retrofit of reinforced concrete beams and columns [4, 5, 6] as well as for masonry [7, 8, 9, 10].

With reference to the latter issue, retrofit of masonry columns by FRP confinement devices has proved to be an efficient strategy, particularly feasible for existing structures [7, 8]. Nevertheless, the design of one-dimensional confined elements is addressed by strategies taking benefit of radial symmetry conditions of the confining stress, such as the Mander's model for confined concrete [9], which holds only for cylindrical confinement.

Recent applications concerning the reinforcement of two-dimensional structural elements have been devoted to characterize confinement effects on stone masonry [10, 11, 12] and brick walls [13], with particular emphasis on the use of Fiber-Reinforced Polymer (FRP) materials as confining devices [14]. Although, in common design practice strength and ductility increment induced by confining devices is accounted for by adopting increased values for the uniaxial failure stress and strain [15]. Such an approach discards both the real multi-axial stress-strain state of plane structural elements [16, 17] as well as the interaction between the confined core of the reinforced elements and the confining devices.

This last aspect is of particular interest since premature failures either of the confining devices or of their anchorages to the core material dramatically compromise the strength capacity of the reinforced elements. In particular, while confinement is easily accounted for by enhancing the mechanical properties of the confined materials, the cyclic behavior of confining material is neglected even for structures subjected to

ACCEPTED MANUSCRIPT

seismic actions.

An important aspect concerning the mutual relationship between the confining devices and the confined core concerns a proper design of the strength of both components. In particular, it is desirable that confining devices are sufficiently resistant to avoid premature failure with respect to the collapse of the confined core. Such a strength hierarchy should prevent dangerous drops of ductility and subsequent fragile collapses, especially in presence of cyclic actions. Actually, as discussed in Section 2, strength of the confining devices, although sufficient from a static point of view, could not be adequate in the case of cyclic loading. For this reason, it is important to develop a proper design rule in order to ensure that the confined core attains its ultimate strength before that confining elements collapse. However, current research has not yet focused on the definition of appropriate strength hierarchy provisions between confined material and confining devices.

Aiming at filling this gap, the present research proposes capacity requirements for confinement devices and their anchorages to the core material. Provisions are derived by simple and reliable theoretical models based on the use of a limited number of constitutive parameters. Hence, two strength hierarchy equations referring to the operative conditions of active and passive confinement are presented in Section 3. Both expressions furnish the minimum yield stress required by confining devices and their anchorages as a functions of the constitutive parameters of the confined core. These conditions are obtained by considering a Drucker-Prager constitutive relationship [18] for the confined material and either an elastic-fragile or an elastic-plastic model for the the confinement devices, which are schematized as transversal one-dimensional ties. Such an approach is based on the finite element formulation of confined shells, proposed in [19, 20], which enforces equilibrium and compatibility conditions along the transversal direction of the confined elements.

The proposed strength hierarchy provisions are discussed in Section 4, where a physical interpretation of the mathematical terms relevant to the proposed expressions is also reported. Moreover, the influence of the constitutive parameters, such as the Poisson's ratio of the confined material and the stiffness of the confining devices, is investigated.

ACCEPTED MANUSCRIPT

The effectiveness of the provided relationships is investigated in Section 5 by means of two numerical applications. Reported results show the behavior of an elementary specimen subject to biaxial static loads and the response of a masonry panel subject to a two-components in-plane ground motion.

Finally, conclusions are drawn in Section 6 where directions of future researches are also discussed.

2. Transverse confinement of shells

Retrofit of existing masonry by transverse confinement usually consists in reinforcing both lateral surfaces of the core masonry by steel or FRP nets protected by a thin concrete casting. In order to provide confinement, lateral reinforcements are connected by transverse links crossing the masonry as shown in Figure 1, where a typical layout of a confining retrofit is presented.

Nowadays a large variety of transverse connections is used in common practice; in particular, steel stirrups are very popular because of their low cost and easy installation and setup. Nevertheless, the use of Fiber-Reinforced Polymer (FRP) ropes, such as the ones shown in Figure 2, has become attractive because of their capability of providing reversible and low-impact retrofits of historic buildings.

In general, regardless of the nature of the tie materials, such devices present a tensile-only behavior since they are barely capable of bearing compressive loads. Actually, the compressive strength of ties is very limited since such slender elements are subject to buckling phenomena and because of the low strength of anchorages subjected to pull-out actions. Therefore, it is reasonable to neglect the compressive contribution of the transverse ties and to assume tensile-only behavior.

Confining action of the transverse ties increases masonry strength and ductility. In particular, it enhances the compressive strength of masonry due to the beneficial effect of the triaxial stress state. Such experimentally observed phenomenon represents the theoretical basis of several strategies that model confinement in concrete and masonry [9] by employing the Drucker-Prager yield criterion [18].

Compressive actions induced by transverse ties can be regarded as concentrated

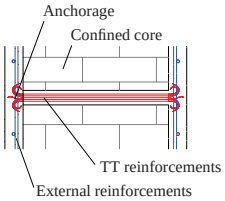

Figure 1: Scheme of a masonry shell confined by Through-the-Thickness ties

Figure 2: *Oly Rope Aramide* Kevlar transverse ties type (courtesy of Olympus srl)

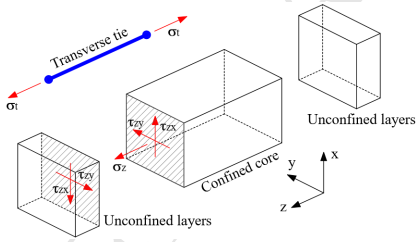

Figure 3: Neighborhood of a masonry chord confined by smeared Through-the-Thickness ties.

loads applied to the core and their effectiveness depends on the actual tie distribution. However, analysis strategies dealing with the real ties distribution are complex and computationally demanding; hence they are not easily used for the analysis real-scale structural models.

To overcome this drawback, a smeared formulation of the confinement effects can be used. Such an approach has been already implemented within a finite element-based algorithm [19, 20] for the analysis of confined shells. Such a strategy analyzes the neighborhood of a shell chord associated with a point P of the shell mid-plane, i.e the plane $x - y$ shown in Figure 3. This neighborhood includes an internal core of thickness δ confined by a uniaxial transverse tie directed along the axis z, orthogonal

ACCEPTED MANUSCRIPT

to the shell mid-plane.

The smeared formulation characterizes the transverse tie by means of the confinement ratio $\mu = \Omega_t/\Omega$ between the area Ω_t of the ties and the total area Ω of the confined shell. In the adopted formulation the presence of external, unconfined, layers is contemplated as well.

Confinement is modelled by means of equilibrium and compatibility conditions enforced by

$$\sigma_z(P,z) + \mu\sigma_t(P) = 0; \quad z = \pm\delta/2 \tag{1}$$

$$\int_{-\delta/2}^{\delta/2} \varepsilon_z(P,z)\, dz = \delta\varepsilon_t(P) \tag{2}$$

respectively.

Equation (1) expresses equilibrium along the z axis and includes the stress component σ_z and the uniaxial stress of the transverse ties σ_t normalized by the confinement area ratio μ. Note that the effect of the stress components τ_{zx} and τ_{zy} has not been included within Eq. (1) since shear stresses associated with FRP or steel ties are negligible with respect to the shear stiffness of the external layers.

Equation (2) enforces compatibility between the tie and the confined core. In particular, assuming a constant uniaxial strain $\varepsilon_t(P)$ of the transverse tie and indicating by $\varepsilon_z(P,z)$ the strain component of the confined core along z, Equation (2) equates the elongation $\delta\varepsilon_t$ of the transverse tie and the stretching of the confined core along z. The latter is computed as the integral of $\varepsilon_z(P,z)$ along the core thickness.

Differently from typical approaches to the analysis of unconfined panels [21, 22, 23], which employ a plane stress assumption, the present formulation considers a triaxial stress state of the confined core accounting for confinement effects. Such an approach has been already been applied to static [19, 20], time-history dynamic [24, 25] and reliability analyses [26, 27] showing that both strength and ductility of non-linear shells are improved by the presence of transverse confinements.

2.1. Degradation of confinement devices under cyclic loading

Dynamic analyses presented in [24] and [25] prompted an issue which did not emerge in static analyses [19] concerning the behavior of the transverse ties. In partic-

ACCEPTED MANUSCRIPT

ular, the presence of several load cycles has shown that the post-yielding behavior of transversal ties can foster a progressive deterioration of the confinement action. Hence, confining devices have to be designed with the goal of avoiding yielding or breakage of these elements.

The importance of a proper design of the transverse ties strength is trivial for the case of elastic-fragile materials such as carbon or kevlar fibers. In fact, the attainment of the maximum strength of the confinement causes failure of the transverse ties or of their anchorage; this compromises confinement of the core material.

For what concerns the employment of elastic-plastic confinement devices, cyclic analyses have shown that yielding of the transverse ties causes cumulative residual strain within these elements. Hence, the right-hand side of the compatibility Equation (2) has to include the cumulated plastic strain within the tie as well. This implies that confinement becomes effective only after that the transverse stretching of the core material recovers such a cumulated plastic strain. This phenomenon can become critical since a reduced confinement can significantly adulterate the behavior of the shell core which, as an extreme consequence, could collapse before that the confinement system becomes effective again.

3. Computation of the transverse ties limit stress

In order to avoid premature crisis of the transverse ties, suitable design boundaries capable of enforcing a strength hierarchy between transverse ties and the confined core are introduced. In particular, stress limit of the ties should be sufficiently high to ensure that shell core can attain its limit state before that failure of the ties compromises the confinement. To this end, it is useful to define the *Transverse Reinforcement Required Strength* (TRRS), denoted by σ_{TT}° and $\sigma_{TT}^{\star}$ for the case of active and passive confinement, respectively, as the minimum value that the stress limit of the transverse confinement system (depending on the strength of the reinforcements and/or of their anchorages) must assume in order not to collapse or yield before that the confined core fails. The values of σ_{TT}° and $\sigma_{TT}^{\star}$ will be estimated below by assuming either an elastic-fragile or elastic-plastic stress-strain relationship characterized by Young's

ACCEPTED MANUSCRIPT

modulus E_s and a stress limit σ_s for the transverse ties. Confined core is assumed to have an elastic-plastic behavior with Young's modulus E_c, Poisson's ratio ν_c and yield condition described by Drucker-Prager limit surface [18]. Such a constitutive model is very popular for modelling multiaxial behavior of existing masonry [28, 29] and requires the determination of a limited set of parameters easily identifiable in practical applications. Hence, it is particularly suitable for the application at hand.

Denoting by σ_1, σ_2 and σ_3 the principal stress components, the Drucker Prager limit surface is defined as:

$$f_l(\boldsymbol{\sigma}) = \frac{\sqrt{(\sigma_1-\sigma_2)^2+(\sigma_2-\sigma_3)^2+(\sigma_3-\sigma_1)^2}}{\sqrt{3}} - \rho I - \sigma_y \leq 0 \tag{3}$$

where $I = (\sigma_1+\sigma_2+\sigma_3)$ is the first stress invariant while σ_y and ρ are constitutive parameters given by:

$$\sigma_y = \frac{2\,|\sigma_c|\,\sigma_t}{|\sigma_c|-\sigma_t} \tag{4}$$

$$\rho = \frac{\sigma_t+|\sigma_c|}{|\sigma_c|-\sigma_t}\sqrt{\frac{2}{3}} \tag{5}$$

σ_c and σ_t denoting the compressive and tensile uniaxial stress limits, respectively.

A stress *cap* defined by

$$f_p(\boldsymbol{\sigma}) = p_y - I \leq 0 \tag{6}$$

is used to introduce a boundary $p_y < 0$ to the spherical stress I. Although several formulations are available in the literature for defining the cap of the Drucker Prager surface [30, 31, 32, 33], we deliberately choose the form of Eq. (6) for the sake of simplicity. Actually, it represents the equation a plane orthogonal to the hydrostatic axis encompassing all the alternative cap formulations.

A geometrical interpretation of the Drucker-Prager criterion can be visualized in the space of principal stress components, having unit basis vectors $\hat{\mathbf{e}}_1$, $\hat{\mathbf{e}}_2$ and $\hat{\mathbf{e}}_3$, see, e.g., Figure 4. Here the yield surface is represented by a blue cone having its axis laying on the hydrostatic axis, which is represented as a black dashed line having unit vector $\hat{\mathbf{i}}$. The circular cross-section of the cone lies in the deviatoric plane which the orthogonal unit vectors $\hat{\mathbf{d}}$ and $\hat{\mathbf{d}}^{\perp}$ belong to, see, e.g. Figure 5.

ACCEPTED MANUSCRIPT

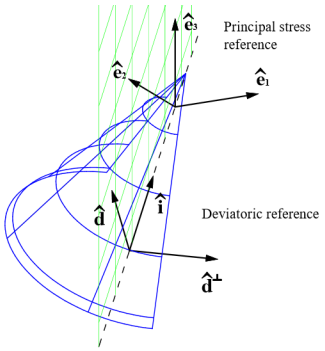

Figure 4: Drucker Prager yield surface and deviatoric reference system represented in the principal stress space

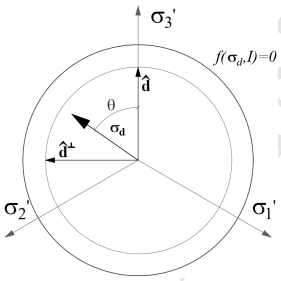

Figure 5: Deviatoric plane and reference system

The unit vectors $\hat{\mathbf{i}}$, $\hat{\mathbf{d}}$ and $\hat{\mathbf{d}}^{\perp}$ have components

$$\hat{\mathbf{i}} = \begin{bmatrix} \frac{1}{\sqrt{3}} \\ \frac{1}{\sqrt{3}} \\ \frac{1}{\sqrt{3}} \end{bmatrix}; \quad \hat{\mathbf{d}} = \begin{bmatrix} \frac{-1}{\sqrt{6}} \\ \frac{-1}{\sqrt{6}} \\ \sqrt{\frac{2}{3}} \end{bmatrix}; \quad \hat{\mathbf{d}}^{\perp} = \begin{bmatrix} \frac{1}{\sqrt{2}} \\ \frac{-1}{\sqrt{2}} \\ 0 \end{bmatrix} \tag{7}$$

so that $\hat{\mathbf{d}}$ is the unit vector obtained by projecting $\hat{\mathbf{e}}_3$ onto the deviatoric plane. The vectors $\hat{\mathbf{i}}$ and $\hat{\mathbf{d}}$ define a plane that contains the hydrostatic axis and the axis σ_3; it is represented by the green grid in Figure 4.

Denoting by σ_d the norm of the stress deviatoric stress $\boldsymbol{\sigma}_d$ and by θ the angle between $\boldsymbol{\sigma}_d$ and $\hat{\mathbf{d}}$, the ith principal stress component can be expressed as a function

ACCEPTED MANUSCRIPT

of I, σ_d and θ as

$$\sigma_i = I/3 + \sigma_d \left[\cos\theta\hat{\mathbf{d}} + \sin\theta\hat{\mathbf{d}}^{\perp}\right] \cdot \hat{\mathbf{e}}_i \qquad i = 1\dots 3 \tag{8}$$

which specializes to

$$\begin{aligned}
\sigma_1 = &\quad I/3 + \sigma_d \left(\frac{1}{\sqrt{2}}\sin\theta - \frac{1}{\sqrt{6}}\cos\theta\right) \\
\sigma_2 = &\quad I/3 - \sigma_d \left(\frac{1}{\sqrt{2}}\sin\theta + \frac{1}{\sqrt{6}}\cos\theta\right) \\
\sigma_3 = &\quad I/3 + \sigma_d\sqrt{\frac{2}{3}}\cos\theta
\end{aligned} \tag{9}$$

This representation of the principal stress components allows one to rewrite the yield condition (3) as:

$$f_l\left(\boldsymbol{\sigma}\right) = \sigma_d - \sigma_y\sqrt{\frac{2}{3}} + \rho I \leq 0 \tag{10}$$

Both yield conditions (6) and (10) are independent from the actual order used to sort the three principal stresses components σ_1, σ_2 and σ_3; hence the three expressions in Eqs. (9) are interchangeable.

The following two sub-section have the objective of providing suitable estimates of the TRRS for the cases of active and passive confinement, respectively. Actually, transversal stresses associated with active confinement devices are commonly defined by the designer, while confining stresses associated with passive confinement devices depend on the transverse stretching of masonry. Hence, these conceptually different confinement techniques require distinct assumptions for a proper derivation of the relevant strength requirements.

3.1. TRRS for active confinement

Active confinement techniques produce additional stress states within the core material introduced by means of post-tensioned confining devices, such as the DIS-CAM system [34], or more traditional Dividag bars and tendons. The additional stress state

ACCEPTED MANUSCRIPT

is superimposed to the one already acting within the confined structural elements and, according to the equilibrium condition (1), the confinement stress σ_t will keep proportional to the core stress component σ_z by means of the confinement area ratio μ.

Due to Equations (6) and (10), Drucker-Prager yield condition imposes a precise limit to the stress values within the confined material. Accordingly, σ_z, or equivalently σ_t, turns out to be limited by the yielding of confined core. This limit value, indicated by σ_z^-, represents the maximum confinement action that the confined core can withstand.

It is worth noting that the above mentioned formulas of the yield surface are expressed in terms of the principal stress components σ_1, σ_2 and σ_3, while the limit stress σ_z^- is the normal stresses orthogonal to the shell mid plane. In general, the stress component σ_z does not coincide with a principal stress due to the presence of tangential components τ_{zy} and τ_{zx}, see, e.g, Figure 3. However, a generic normal stress $\sigma_{\hat{\mathbf{n}}}$, computed on a plane of unit normal $\hat{\mathbf{n}}$, always fulfils the condition:

$$\min(\sigma_1, \sigma_2, \sigma_3) \leq \sigma_{\hat{\mathbf{n}}} \leq \max(\sigma_1, \sigma_2, \sigma_3) \quad \forall \hat{\mathbf{n}}$$

Thus, being σ_z^- the absolute maximum compressive stress acting on the confined core, it must coincide with the lower principal stress component. Accordingly, when such a limit is attained, z becomes a principal stress direction and $\sigma_z = \mu\sigma_t = \sigma_z^-$ is the corresponding principal stress.

Employing the third formula in Eq. (9) to express such a principal stress value, the theoretical boundary of the transverse stress can be determined by minimizing σ_3 for all possible values of I, σ_d and θ. It is easy to verify that such a minimum is attained when both yielding conditions (10) and (6) are fulfilled with the equal sign and $\cos\theta = -1$; hence

$$\sigma_z^- = \min(\sigma_3) = \frac{p_y}{3} - \frac{2}{3}\sigma_y + p_y\rho\sqrt{\frac{2}{3}} \tag{11}$$

Therefore, the corresponding hierarchy condition for the active-confinement TRRS stress σ_{TT}° is

$$\mu\sigma_s \geq \sigma_{TT}^\circ = \frac{2}{3}\sigma_y + |p_y|\left(\frac{1}{3} + \rho\sqrt{\frac{2}{3}}\right) \tag{12}$$

ACCEPTED MANUSCRIPT

where σ_s denotes the limit stress of transverse ties.

Note that condition (11) has been obtained by employing only equilibrium and yield conditions. Although conservative, it represents the ultimate value that the compressive stress can reach within the confined core. Therefore, Equation (12) represents a physical boundary for the stress acting in the transverse ties regardless of the actual stress state associated with the confined core.

3.2. TRRS for passive confinement

The theoretical boundary of the transverse stress computed by Equation (12) turns out to be excessively conservative for the case of passive confinement. Actually, in this case, transversal stress is generated by the contrast between the confining device and the lateral expansion associated with the Poisson effect in the confined core. Hence, for passively confined shells, the value of the transverse stress does depend upon the actual stress state acting within the confined core.

Differently from the TRRS computed for active confinements, the limit stress associated with passive confinement devices also depends upon the compatibility condition (2) which is used to express the contrast between taut ties and expanding confined core. Assuming that stresses within the confined core and within the transverse ties lay in the elastic range, the transversal strain associated with these structural elements is computed as

$$\begin{aligned} \varepsilon_t = &\quad \frac{\sigma_t}{E_s} \\ \varepsilon_z = &\quad \frac{\sigma_z}{E_c} - \frac{\nu_c}{E_c}\left(\sigma_x + \sigma_y\right) \end{aligned} \tag{13}$$

where dependence upon P has been omitted for brevity. Here, E_s represents the Young's modulus of the transverse ties while E_c and ν_c are the Young's modulus and the Poisson's ratio of the shell core material, respectively. Equations (13) are used in (2) which is then solved for σ_t. The resulting expression of σ_t is then used within the equilibrium Equation (1), yielding:

$$-\frac{\sigma_z}{\mu E_s} = \frac{\sigma_z}{E_c} - \frac{\nu_c}{E_c}\left(\sigma_x + \sigma_y\right) \tag{14}$$

ACCEPTED MANUSCRIPT

where dependence upon P has been omitted for brevity.

Stress components in (14) are required to fulfil the Drucker Prager limit conditions expressed by Eqs. (3) and (6). These conditions are written in terms of pricipal stress components, while Eq. (14) contains the normal stress components referred to the Cartesian reference frame laying in the shell mid-plane, where also the shear stress components τ_{zy} and τ_{zx} are present (see, e.g., Fig. 3). However, the maximum stress within passive ties is activated when the core material expands constantly along the transversal direction. This happens when σ_3 is constant along the shell chord so that, by equilibrium, $\tau_{zy} = \tau_{zx} = 0$. Incidentally, this phenomenon has been already pointed out in [19], where it has been shown how the highest effect of transversal confinement is achieved when the shell is subjected to in-plane loadings.

Accordingly, for estimating the maximum tensile stress activated in the ties by the transversal elongation of the confined core, it is conservative to assume that z is a principal direction of the stress. Thus, the remaining two principal stress directions and the relative principal stresses, namely σ_1 and σ_2, lay onto the shell mid-plane. As a result, Eq. (14) can be rewritten as

$$\sigma_z = \frac{\mu E_s \nu_c}{\mu E_s + E_c} (\sigma_1 + \sigma_2) \tag{15}$$

Employing he first two formulas in Eq. (9) to express σ_1 and σ_2 as a function of the hydrostatic and deviatoric stress norms, Eq. (15) becomes

$$\sigma_z = \frac{\mu E_s \nu_c}{\mu E_s + E_c} \left[\frac{2}{3} I - \frac{2}{\sqrt{6}} \sigma_d \cos(\theta) \right] \tag{16}$$

The TRRS of the passive confining ties is attained when σ_z reaches its global minimum, i.e. when $\cos(\theta) = 1$ and when both yielding conditions (10) and (6) are fulfilled with the equal sign. Accordingly, one has

$$\sigma_z^- = \frac{\mu E_s \nu_c}{\mu E_s + E_c} \left[\frac{2}{3} p_y + \frac{2}{\sqrt{6}} \rho I - \frac{2}{3} \sigma_y \right] \tag{17}$$

ACCEPTED MANUSCRIPT

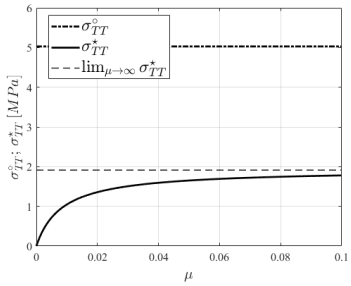

Figure 6: Transverse Reinforcement Required Strengths σ°_{TT} and $\sigma^{\star}_{TT}$ as functions of the confinement area ratio μ

and the passive-confinement Transverse Reinforcement Required Strength is:

$$\mu\sigma_s \geq \sigma^{\star}_{TT} = \frac{2}{3}\frac{\mu E_s \nu_c}{\mu E_s + E_c}\left[\sigma_y + |p_y|\left(1+\rho\sqrt{\frac{3}{2}}\right)\right] \tag{18}$$

which enforces yielding of the internal core before collapse of the passive confinement system.

4. Physical interpretation of the Transverse Reinforcement Required Strength

Stress boundaries σ°_{TT} and $\sigma^{\star}_{TT}$ provided by Equations (12) and (18) ensure that transverse ties and their anchorages do not yield nor fail before than the confined core so as to avoid fragile collapse. However these limits attain different values due to the different technology of confinement they refer to.

The limiting value σ°_{TT} depends on the maximum stress that the core material can bear regardless of the physical confinement mechanism that induces the stress state. In fact, the ratio of the active confinement consists in imposing an additional and arbitrary stress state by applying post-tensioned devices. Expression of σ°_{TT} in Eq. (12), although dependent on the yield parameters of the internal core, is not influenced by its stiffness parameters E_c and ν_c.

On the contrary, the boundary $\sigma^{\star}_{TT}$, referring to passive confinement, is a function of the core stiffness parameters since tensioning of the confining reinforcements is generated by the transversal dilatation strain of the confined core.

ACCEPTED MANUSCRIPT

In order to understand the physical meaning of these two strength requirements, it is useful to plot σ°_{TT} and $\sigma^{\star}_{TT}$ versus the ratio μ, see, e.g., Figure 6. These curves have been computed by assuming a masonry core having constitutive parameters $E_c = 900\,MPa$, $\nu_c = 0.3$ and yielding parameters $\sigma_c = -1.4\,MPa$, $\sigma_t = 0.14\,MPa$ and $p_y = -4.2\,MPa$. Such values correspond to a rubble stone masonry characterized by the prescriptions of the Italian Structural Code [35]. Transverse ties are characterized by $E_s = 107\,GPa$ and $\sigma_s = 1574\,MPa$ corresponding to the Kevlar cable *Oly Rope Aramide* manufactured by the Olympus Srl.

As expected, σ°_{TT} is significantly greater than $\sigma^{\star}_{TT}$ and does depend neither upon the area of the confinement ties nor upon the value of the material constitutive parameters. Moreover, its value is higher then the limit hydrostatic pressure p_y of the confined core.

Conversely, $\sigma^{\star}_{TT}$ depends both on the yield conditions and the elastic parameters of materials. Consistently with the concept of passive confinement, $\sigma^{\star}_{TT}$ is directly proportional to the Poisson ratio of the core material, meaning that passive confinement stresses are explicitly activated by the transversal elongation of shell chords generated by in-plane stresses. It exhibits a monotonic dependence on the area ratio μ with an asymptotic trend for increasing values of μ. When transverse ties are absent, i.e. when $\mu = 0$, the shell core is free to expand along the transversal direction, the stress state within the shell is planar with $\sigma_z = 0$, and null strength is required for confining ties. The asymptotic value of $\sigma^{\star}_{TT}$ can be easily computed from Equation (18) by evaluating the limit:

$$\lim_{\mu\to\infty} \sigma^{\star}_{TT} = \frac{2}{3}\frac{E_s\nu_c}{E_s + E_c}\left[p_y\left(1 + \rho\sqrt{\frac{3}{2}}\right) + \sigma_y\right] \tag{19}$$

As expected, such an asymptotic value does not depend on μ and it is significantly smaller than the value of σ°_{TT} computed for the same materials.

It is worth pointing out that Equation (18) is not defined when $\mu = -E_c/E_s$ since the denominator vanishes in this case. Such a critical value of μ corresponds to a vertical asymptote for $\sigma^{\star}_{TT}$, laying on the negative part of the μ axis, which is physically unfeasible. However, this observation suggests the fact that the relationship between $\sigma^{\star}_{TT}$ and μ is described by an hyperbole centred at the crossing between these two

ACCEPTED MANUSCRIPT

asymptotes. Actually, rewriting Equation (18) by setting:

$$\bar{\mu} = \mu + E_c/E_s \tag{20}$$

and:

$$f\left(\bar{\mu}\right) = \sigma_{TT}^{\star} - \frac{2\nu_c}{3}\left[p_y\left(1+\rho\sqrt{\frac{3}{2}}\right)+\sigma_y\right] \tag{21}$$

one has:

$$f\left(\bar{\mu}\right) = \overbrace{-\frac{2}{3}\frac{E_s E_c \nu_c}{{E_s}^2}\left[p_y\left(1+\rho\sqrt{\frac{3}{2}}\right)+\sigma_y\right]}^{\text{constant}}\frac{1}{\bar{\mu}} \tag{22}$$

representing the canonic equation of an equilateral hyperbola in the $[\bar{\mu},\ f\left(\bar{\mu}\right)]$ plane.

5. Numerical application

In order to show the effectiveness of the proposed provisions, the results of two numerical analyses are reported in the sequel. The first example regards a square masonry panel, subjected to a monotonic load, for which the local behavior of the yield functions and the effectiveness of the strength hierarchy condition provided by Equation (18) are investigated. A further analysis, consisting of a masonry wall subject to in-plane base excitation, aims at evaluating the evolution of the confinement stress under cyclic loads.

Both structures have been modelled by employing the MITC-TTJS shell element formulation described in [19, 20] in order to include transverse reinforcements. An elastic-plastic constitutive law characterized by a Young modulus $E_c = 900\,MPa$ and a Poisson's ratio $\nu_c = 0.3$ has been assumed for the shell core. A Drucker Prager yield criterion characterized by compressive $\sigma_c = -1.4\,MPa$ and tensile yield stress $\sigma_t = 0.14\,MPa$, respectively, and by the hydrostatic limit stress $p_y = -4.2\,MPa$ has been selected. These parameters are consistent with the ones prescribed by the Italian Structural Code [35] for rubble stone masonry. Transverse reinforcements are characterized by $E_s = 107\,GPa$, which corresponds to a Kevlar cable *Oly Rope Aramide* manufactured by the Olympus Srl.

ACCEPTED MANUSCRIPT

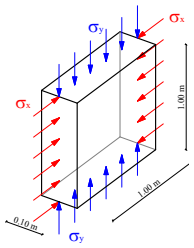

Figure 7: Model of the masonry panel analyzed by a static monotonic test

5.1. Square panel subjected to a static monotonic test

The first structural model consists of a series of $1\,m \times 1\,m$ square panels having thickness $0.1\,m$ and confined by transversal ties characterized by different values of the area ratio μ, respectively equal to 0.001, 0.005, 0.01, 0.05 and $+\infty$. These panels are subjected to uniformly distributed compressive normal stresses σ_x and σ_y acting in the plane of the panel, see, e.g., Figure 7. Static non linear analyses have been performed by applying a displacement driven incremental procedure in which the strain ε_x has been selected as control parameter and has been increased until the attainment of a yield condition for the core material. Four sets of analyses have been conducted for each panel by varying the value of the ratio σ_y/σ_x, which has been set equal to 0, 0.05, 0.25 and 1.00 for each analysis. Because of the symmetry of the Drucker Prager yield surface, the role played by σ_x and σ_y is interchangeable so that there is no need to consider value of σ_y/σ_x greater then 1. Also, due to the limited strength of the core material with respect to tensile actions, the employment of negative values of the ratio σ_y/σ_x produces premature yielding of the core material. Hence such situations are irrelevant for testing the effectiveness of the proposed TRRS value.

The results of this first set of analyses are reported in Figure 8 where the value of the ratio between the transverse stress $\sigma_z = \mu\sigma_s$ and its limit value $\sigma^{\star}_{TT}$, computed by Equation (18), is plotted versus the maximum between the two yield functions f_l and f_p relevant to the lateral surface and to the cap of the Drucker Prager domain, respectively. In the same figures, vertical and horizontal black dashed lines indicate the attainment of the yield condition for the core material and of the TRRS for the confinement ties, respectively.

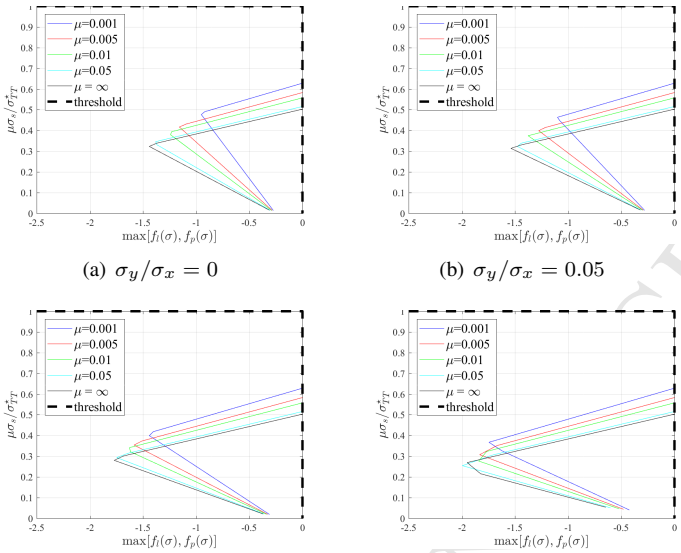

(a) $\sigma_y/\sigma_x = 0$ (b) $\sigma_y/\sigma_x = 0.05$

(c) $\sigma_y/\sigma_x = 0.25$ (d) $\sigma_y/\sigma_x = 1.00$

Figure 8: Transverse stress ratio vs. maximum yield function $\max\left[f_l(\boldsymbol{\sigma}),\ f_p(\boldsymbol{\sigma})\right]$

Firstly, it is worth noting that all plotted paths are represented by two straight lines characterized by negative and positive slopes, respectively. This is consistent with the assumption of a yield surface characterized by two expressions, reported in Eqs. (6) and (10), which are linearly dependent upon the first stress invariant I. Actually, the presented analyses are relevant to a progressive increment of both the stress components σ_x and σ_y. As a consequence, the transversal normal stress $\sigma_z = \mu\sigma_s$ also increases because of the transversal confinement. The corresponding value of I increases as well and directly influences the value attained by the stress functions $f_l(\boldsymbol{\sigma})$ and $f_p(\boldsymbol{\sigma})$. In particular, while for lower values of I the value of the stress function $f_l(\boldsymbol{\sigma})$ is closer than $f_p(\boldsymbol{\sigma})$ to the yield condition, the opposite happens when I is higher. Hence, the lower branches of the stress paths shown in all plots of Figure 8 correspond to stress states for which $f_l(\boldsymbol{\sigma}) > f_p(\boldsymbol{\sigma})$ while successive branches are relevant to cases in which $f_l(\boldsymbol{\sigma}) < f_p(\boldsymbol{\sigma})$.

As a matter of fact, all paths are located below the threshold line $\mu\sigma_s/\sigma^{\star}_{TT} = 1$, meaning that the value of the transverse stress is always smaller than the corresponding

TRRS. This is consistent with the hypothesis underlying the derivation of Equation (18) which inhibits yielding of transversal ties before that of the confined core. This numerically confirms the effectiveness of the proposed strength hierarchy rule.

5.2. Masonry wall subjected to base excitation

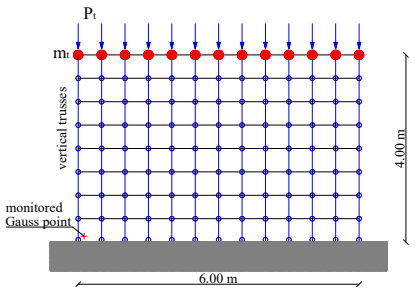

Figure 9: Mesh of the masonry wall subject to vertical loads and in-plane base excitation

In order to show the effectiveness of the provided strength hierarchy relationships when the confined shell is subjected to real conditions, the results of a further numerical example are reported hereafter. The test reproduces a typical retrofit intervention for historical masonry where transverse confinement is used in conjunction with vertical post-tensioned tendons.

The wall is schematized in Figure 9 and consists of a $6\,m \times 4\,m$ masonry wall of thickness $0.8\,m$, discretized by a mesh of 12×8 shell elements, fully constrained at the base edge. Transversal confinement has been modelled by adopting the Through-

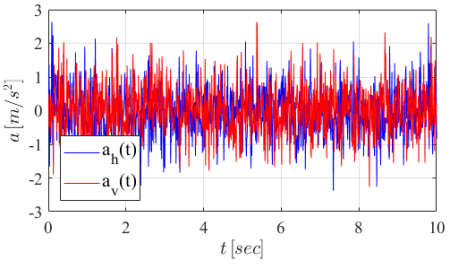

Figure 10: White-noise Base excitation used in the dynamic analysis

ACCEPTED MANUSCRIPT

The-Thickness Jacketed Shell (TTJS) finite element formulation presented in [19, 20], already used in the previous example. Vertical reinforcement has been modelled by including vertical truss elements which superimpose to the shell mesh. These elements are represented by the vertical blue lines in Fig. 9.

The wall material has density $w = 2000\,kg/m^3$. However, additional masses have been applied to the nodes at the top of the model so as to simulate the presence of a deck. These nodal masses have been computed by considering a line mass equal to $m_t = 6000\,kg/m$ uniformly distributed along the top edge of the wall.

Mechanical properties of the core material are defined in accordance to the Italian structural code [35] and are relevant to rubble-stone masonry with Young's modulus $E_c = 1.26 \cdot 10^3\,MPa$, Poisson's ratio $\nu_c = 0.45$ and uniaxial compressive strength $\sigma_c = -1.0\,MPa$. It has been modelled by means of an elastic-perfectly plastic Drucker-Prager constitutive law with parameters $\sigma_y = 2.22 \cdot 10^{-1}\,MPa$, $\rho = 0.998$ and $p_y = -5.0\,MPa$. A uniaxial tensile-only linear elastic constitutive behavior with Young's modulus $E_s = 1.07 \cdot 10^5\,MPa$ relevant to connectors type *Oly Rope Aramide* manufactured by *Olympus s.r.l.* has been used to model transverse confining devices. The same five values of the transverse area ratio μ already considered in the previous example have been employed for the case at hand so as to produce five different models. Vertical reinforcements are characterized by a linear-elastic uniaxial material with Young's modulus $E_t = 6.0 \cdot 10^4\,MPa$ and circular cross section having diameter $\phi_t = 8\,mm$, relevant to kevlar-fiber pultrued bars (type *Oly Rod Aramide* manufactured by *Olympus s.r.l.*).

The weight of the deck is modelled by applying nodal forces to the nodes of the wall's top edge. Their values have been estimated by considering a vertical load equal to gm_t, $g = 9.81\,m/s^2$ being the gravitational acceleration, uniformly distributed on the top edge of the model. Additionally, in order to account for post-tensioning of the vertical bars, top nodes are subjected to an additional vertical force equal to $4.0 \cdot 10^5\,N$, which corresponds to a stress increment of $0.4\sigma_c$ at the base of the panel.

The model is subjected to a dynamic excitation lasting $10\,s$ and acting along both vertical and in-plane horizontal directions. Recalling the mechanical behaviors of the confined walls highlighted in [19], the out-of-plane component of the dynamic excita-

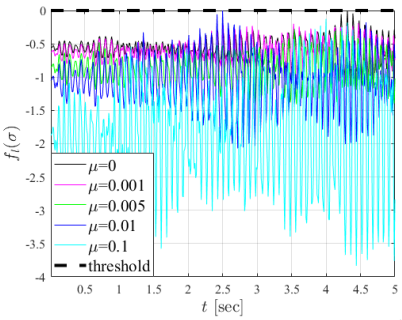

Figure 11: Lateral surface yield function

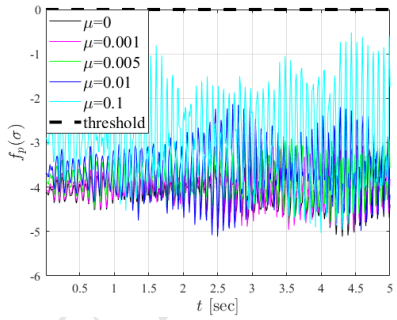

Figure 12: Hydrostatic pressure yield function

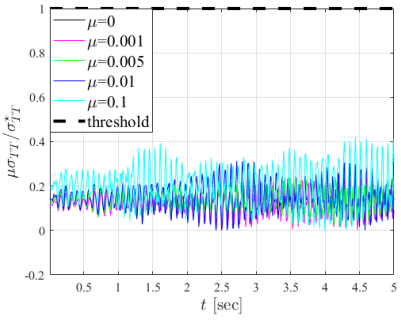

Figure 13: Limit state function of transverse reinforcements

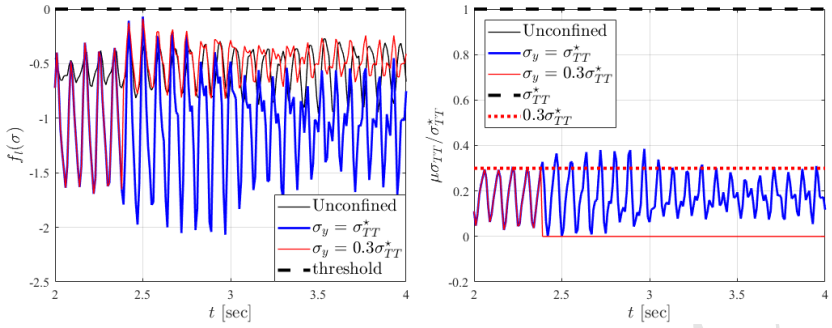

(a) Lateral surface yield function (b) Limit state of transverse reinforcements

Figure 14: Limit state functions of the cyclic analysis with elastic-fragile transverse ties

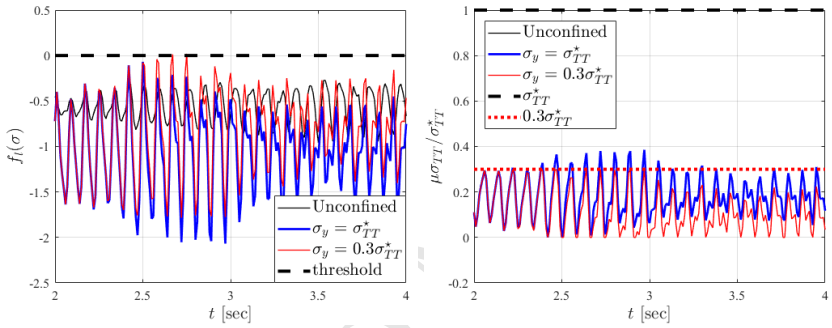

(a) Lateral surface yield function (b) Limit state of transverse reinforcements

Figure 15: Limit state functions of the cyclic analysis with elastic-plastic transverse ties

tion has been intentionally neglected in order to maximize stresses within transversal ties.

The two components of the dynamic load correspond to banded white-noise stationary accelerograms having constant power spectral density of intensity $\Phi_0 = 4.5 \cdot 10^{-6} g^2$. They are shown in Figure 10 by the curves a_h and a_v, respectively referred to the horizontal in-plane and the vertical acceleration components. Accelerograms have been discretized by adopting time steps $\Delta t = 0.01\, s$ and determining a band cutoff at the frequency $f_{co} = \pm 0.5 \Delta t^{-1} = 50\, Hz$. The two acceleration components a_h and a_v, represented in Figure 10, are oriented along the horizontal and vertical dimension of the wall, respectively.

Results of the dynamic analysis are relevant to a monitored Gauss point positioned

ACCEPTED MANUSCRIPT

at the lower-left corner of the structural model. It has been selected as the Gauss point where higher values of stress are expected and is indicated by the red cross shown in Figure 9.

Figures 11-13 refer to the value of the yield functions computed for the core material and the transverse ties by considering all mentioned values of the transverse area ratio μ. The black dashed lines represent the threshold value of the yield functions: points lying above the threshold are physically unacceptable. In particular, Figure 11 reports the time variation of the yield function $f_l(\boldsymbol{\sigma})$ in Equation (10), which is relevant to the lateral conic portion of the yield surface, while Figure 12 corresponds to the hydrostatic pressure yield function $f_p(\boldsymbol{\sigma})$, defined by Equation (6).

It is worth pointing out that Figure 11 shows that, for lower values of the confinement area ratio μ, the distance between the yield function $f_l(\boldsymbol{\sigma})$ is higher, hence closer to the threshold value. On the contrary, the values of the yield function $f_p(\boldsymbol{\sigma})$, reported in Figure 12, turn out to become closer to the threshold as long as the confinement area ratio μ increases. This different behavior is due to the fact that higher values of μ correspond to stiffer transverse reinforcement and, hence, higher values of confinement stress. This produces higher values of I so that the stress state within the confined core moves towards regions of the yield domain which are closer to the stress cap. Therefore, $f_p(\boldsymbol{\sigma})$ increases while $f_l(\boldsymbol{\sigma})$ decreases because the Drucker-Prager cone becomes wider.

Ratios between the computed stress in transversal reinforcements, computed as $\mu\sigma_t$, and the TRRS $\sigma^{\star}_{TT}$ are plotted in Figure 13 for each time step of the analysis. The mentioned ratio $\mu\sigma_t/\sigma^{\star}_{TT}$ always keeps lower than 1, meaning that the computed stress within confining devices is always smaller than their prescribed strength $\sigma^{\star}_{TT}$. This happens for all considered area ratios, with a maximum when $\mu = 0.001$; actually, in such a case, the computed confining stress reaches values corresponding to about the 50% of the theoretical limit. This aspect confirms that the proposed estimate of $\sigma^{\star}_{TT}$ is safe and consistent with more accurate numerical predictions.

In order to investigate the behavior of the considered specimen when the strength of the confining devices is lower than the proposed TRRS, two additional analyses of the same model have been performed by assuming either an elastic-fragile or an elastic-

ACCEPTED MANUSCRIPT

plastic behavior of the confinement devices, respectively. In both the cases, the results of three different assumptions have been compared

a unconfined wall, modeled by assuming $\mu = 0$;

b wall confined by transversal ties fulfilling the proposed TRRS, modeled by assuming $\mu = 0.01$ and setting $\sigma_y = \sigma^{\star}_{TT}$ as strength of the transverse ties;

c wall confined by under-dimensioned transversal ties, modeled by assuming $\mu = 0.01$ and assigning a strength of the transverse ties equal to $\sigma_y = 0.3\,\sigma^{\star}_{TT}$.

Results relevant to the cases of elastic-fragile and elastic-plastic confinement devices are respectively reported in Figures 14 and 15. Plots show the value attained by the yield function $f_l(\boldsymbol{\sigma})$ and by the exploitation ratio $\mu\sigma_t/\sigma^{\star}_{TT}$ for each time step of the analysis and for each of the mentioned three assumptions regarding transverse confinement.

As expected, before the collapse of the confinement devices, the curves relevant to under-dimensioned transversal ties superimposes to the one corresponding to a well-designed confinement. However, as soon as the transversal stress reaches the limit value $\mu\sigma_t/\sigma^{\star}_{TT} = 0.3$, which is represented by the red dotted line in Figures 14(b) and 15(b), the curves relevant to the under-dimensioned transversal ties diverge from those relevant to the well designed confinement.

When under-dimensioned ties obey to an elastic-fragile constitutive behavior, transverse stress immediately drops to zero, see, e.g., Figure 14(b), and the confinement becomes inactive. At the same time, stress state within the core material and the corresponding value of the yield function $f_l(\boldsymbol{\sigma})$ modifies by getting closer to the curve corresponding to the unconfined specimen, see, e.g, Figure 14(a).

Such an abrupt change of behavior is mitigated by the plastic behavior of the confining devices. Actually, as shown in Figure 15(b) for the case of elastic-plastic confinement devices, the attainment of the limit $\mu\sigma_t/\sigma^{\star}_{TT} = 0.3$ does not corresponds to a sudden drop of the transversal stress. Hence, elastic-plastic transversal ties continue to confine the internal core even after yielding, yet with a lower efficiency. This is also shown by Figure 15(b) where the curve corresponding to under-dimensioned ties ex-

ACCEPTED MANUSCRIPT

hibits a behavior which is intermediate between that corresponding to a well designed confinement and the one relevant to an unconfined wall.

5.3. Discussion

Numerical results have proved the effectiveness of the theoretical stress boundary defined in Eq. (18). This is not surprising, especially for the case regarding the static test described in Subsection 5.1. Actually, the application of monotonic load paths produces effects which are very adherent to the assumptions underlying the theoretical derivation of the confinement stress boundary. The dynamic analyses reported in Subsection 5.2 are more significant for real applications. Indeed, even in this last case, the value of the confining stress remains far below the theoretical boundary regardless of the confinement ratio. However, an important remark concerns the conservative nature of the computed theoretical boundary, what is imputable to different reasons.

A first issue concerns the assumption regarding the contemporary attainment of both yield conditions (3) and (6) for the derivation of Equation (18). Although conservative, this condition is rather unlike to occur. A further aspect concerns the assumption regarding the stress state within the confined core, which, for the sake of safety, has been assumed to be subjected to in-plane actions. In most cases, the actual stress state within the confined core is likely to have an out-of-plane component as well.

While this latter assumption depends on the loading conditions, so that it cannot be addressed by a general hierarchy condition based only on material properties, the mutual correlation between the two considered yield functions can be dealt with by assuming different and more refined yield conditions. Nevertheless, complex constitutive models often require a larger amount of mechanical parameters than the Drucker Prager yield condition adopted in this work. Hence, although extensions to different constitutive models can be investigated, the present research aims to provide a simple relationship based on theoretical concepts familiar to the majority of designers and requiring a limited set of parameters easy to derive in common practice. For this reason, the hypotheses adopted for the derivation of the TRRS seem the most immediate and reliable at the present stage of the research. Nevertheless, further investigations are worth being performed concerning the influence of more refined constitutive models.

ACCEPTED MANUSCRIPT

6. Conclusions

The present research has investigated the behavior of transverse reinforcements in plane elements retrofitted by through-the-thickness confinement devices. Two hierarchy conditions have been proposed aiming to define peak values of the confinement stress so that yielding and/or failure of the transverse reinforcements and of their anchorages will not forestall the crisis of the confined material.

Such a requirement is of particular importance when transverse confinement is used in retrofitting structures subjected to seismic loads since the design of transverse reinforcements is often performed by static procedure that disregard the cyclic nature of seismic responses. In particular, the establishment of a strength hierarchy between reinforcements and confined core avoids the possibility that confining devices, although adequate during the first loading of the structural members, becomes ineffective for the remaining loading cycles.

The proposed provisions consists of two relationships. The first condition determines the maximum value of the out-of-plane stress component acting in the confined material. Such a condition is oriented to retrofit interventions presenting post-tensioning of the transverse reinforcements. The second provision, relevant to the case of passive confinement, determines the maximum value of the confinement stress which can be attained by enforcing equilibrium and compatibility conditions between the confined material and the confining devices.

The proposed provisions have been based on a few mechanical parameters familiar to the majority of designers and usually adopted in common practice. Actually, both hierarchy conditions have been derived by assuming an elastic-plastic behavior of the confined material, obeying to a Drucker Prager yield condition, and considering linearly elastic confining devices. Additionally, the results of significant numerical tests have been reported to prove the effectiveness of the proposed formulation so that, although conservative, these provisions are suitable to be used in structural design in order to ensure a proper strength hierarchy of the confinement setup.

Future research activities will focus on the extension of the proposed approach to more refined constitutive models in order to obtain provisions more coherent with

ACCEPTED MANUSCRIPT

the mechanical behavior of materials, such as existing masonry, for which transverse confinement has become a popular retrofit strategy. Moreover, future developments will be focused on the setup of experimental tests oriented to investigating the actual behavior of confinement devices.

Funding and acknowledgments

This work was supported by the Italian Government, ReLuis 2017 project [AQ DPC/ReLUIS 2014-2018, PR2, Task 2.3] and PRIN 2015 grants [2015JW9NJT-PE8, WP2 Task 2.1]. Authors gratefully acknowledge the Olympus srl for its technical support.

References

[1] V. Palazzo, L. Rosati, N. Valoroso, Solution procedures for J3 plasticity and viscoplasticity, Computer Methods in Applied Mechanics and Engineering 191 (8) (2001) 903–939.

[2] G. Alfano, L. Rosati, A general approach to the evaluation of consistent tangent operators for rate-independent elastoplasticity, Computer Methods in Applied Mechanics and Engineering 167 (1-2) (1998) 75–89.

[3] S. Sessa, F. Marmo, L. Rosati, L. Leonetti, G. Garcea, R. Casciaro, Evaluation of the capacity surfaces of reinforced concrete sections: Eurocode versus a plasticity-based approach, Meccanica 53 (6) (2018) 1493–1512.

[4] A. Borri, G. Castori, M. Corradi, Masonry columns confined by steel fiber composite wraps, Materials 4 (2011) 311–326.

[5] N. Nisticó, R.c. square sections confined by FRP: A numerical procedure for predicting stress-strain relationships, Composites Part B: Engineering 59 (2014) 238 – 247.

[6] T. Trapko, Stress-strain model for FRCM confined concrete elements, Composites Part B: Engineering 45 (1) (2013) 1351 – 1359.

ACCEPTED MANUSCRIPT

[7] M. Corradi, A. Grazini, A. Borri, Confinement of brick masonry columns with CFRP materials, Composites Science and Technology 57 (2007) 1772–1783.

[8] T. Ozbakkaloglu, J. C. Lim, Axial compressive behavior of FRP-confined concrete: Experimental test database and a new design-oriented model, Composites Part B: Engineering 55 (2013) 607 – 634.

[9] J. B. Mander, M. J. N. Priestley, R. Park, Theoretical stress–strain model for confined concrete, Journal of Structural Engineering 114 (8) (1988) 1804–1826.

[10] M. Corradi, A. Borri, G. Castori, R. Sisti, Shear strengthening of wall panels through jacketing with cement mortar reinforced by GFRP grids, Composites Part B: Engineering 64 (2014) 33 – 42.

[11] F. F. Pinho, V. J. Lúcio, M. F. Baião, Rubble stone masonry walls strengthened by three-dimensional steel ties and textile-reinforced mortar render under compression and shear loads, International Journal of Architectural Heritage 9 (7) (2015) 844–858.

[12] F. Pinho, V. LÃºcio, M. BaiÃ£o, Experimental analysis of rubble stone masonry walls strengthened by transverse confinement under compression and compression-shear loadings, International Journal of Architectural Heritage 12 (1) (2018) 91–113.

[13] M. Valluzzi, F. Da Porto, C. Modena, Behavior and modeling of strengthened three-leaf stone masonry walls, Materials and Structures 37 (3) (2004) 184–192.

[14] D. V. Oliveira, R. A. Silva, E. Garbin, P. B. Lourenço, Strengthening of three-leaf stone masonry walls: an experimental research, Materials and Structures 45 (8) (2012) 1259–1276.

[15] DM 14 Gennaio 2008, Norme tecniche per le costruzioni, Tech. rep., Min. delle Infrastrutture (2008).

[16] N. Valoroso, F. Marmo, S. Sessa, Limit state analysis of reinforced shear walls, Engineering Structures 61 (2014) 127 – 139.

ACCEPTED MANUSCRIPT

[17] N. Valoroso, F. Marmo, S. Sessa, A novel shell element for nonlinear pushover analysis of reinforced concrete shear walls, Bulletin of Earthquake Engineering 13 (8) (2015) 2367–2388.

[18] D. C. Drucker, W. Prager, Soil mechanics and plastic analysis for limit design, Quarterly of Applied Mathematics 10 (2) (1952) 157–165.

[19] S. Sessa, R. Serpieri, L. Rosati, A continuum theory of through-the-thickness jacketed shells for the elasto-plastic analysis of confined composite structures: Theory and numerical assessment, Composites Part B: Engineering 113 (2017) 225 – 242.

[20] R. Serpieri, S. Sessa, L. Rosati, A MITC-based procedure for the numerical integration of a continuum elastic-plastic theory of through-the-thickness-jacketed shell structures, Composite Structures 191 (2018) 209–220.

[21] N. Valoroso, L. Rosati, Computational analysis of isotropic plasticity models, Lecture Notes in Applied and Computational Mechanics 23 (2005) 173–200.

[22] N. Valoroso, L. Rosati, Consistent derivation of the constitutive algorithm for plane stress isotropic plasticity. Part I: Theoretical formulation, International Journal of Solids and Structures 46 (1) (2009) 74 – 91.

[23] N. Valoroso, L. Rosati, Consistent derivation of the constitutive algorithm for plane stress isotropic plasticity. Part II: Computational issues, International Journal of Solids and Structures 46 (1) (2009) 92 – 124.

[24] S. Sessa, R. Serpieri, L. Rosati, Dynamic FEM analysis of composite shell structures subject to Through-the-Thickness confinement, in: Proc. 3rd International Conference on Mechanics of Composites (MECHCOMP3), 4-7 July 2017, Bologna, Italy, 2017.

[25] S. Sessa, R. Serpieri, L. Rosati, Implementation and finite-element analysis of shell elements confined by Through-the-Thickness uniaxial devices, in: Proc. 1st European Conference on OpenSees, 19-20 June 2017, Porto, Portugal, 2017.

ACCEPTED MANUSCRIPT

[26] R. Serpieri, S. Sessa, L. Rosati, Seismic reliability assessment of historical masonry structures retrofitted with through-the-thickness confinement techniques, in: C. Bucher, B. R. Ellingwood, D. M. Frangopol (Eds.), Safety, Reliability, Risk, Resilience and Sustainability of Structures and Infrastructure. Proc. 12th International Conference on Structural Safety & Reliability (ICOSSAR2017), 6-10 August 2017, Vienna, Austria, 2017.

[27] S. Sessa, R. Serpieri, L. Rosati, Probabilistic assessment of historical masonry walls retrofitted with through-the-thickness confinement devices, in: AIMETA 2017 - Proceedings of the 23rd Conference of the Italian Association of Theoretical and Applied Mechanics, Vol. 3, 2017, pp. 2324–2332.

[28] P. B. Lourenço, J. G. Rots, J. Blaauwendraad, Two approaches for the analysis of masonry structures: micro and macro–modeling, HERON 40 (4) (1995) 313–340.

[29] P. B. Lourenço, Computations on historic masonry structures, Progress in Structural Engineering and Materials 4 (3) (2002) 301–319.

[30] I. S. Sandler, F. L. DiMaggio, G. Y. Baladi, Generalized cap model for geological materials, ASCE J Geotech Eng Div 102 (7) (1976) 683–699.

[31] E. Mizuno, W. Chen, Cap models for clay strata to footing loads, Computers and Structures 17 (4) (1983) 511–528.

[32] M. Katona, Evaluation of viscoplastic cap model, Journal of Geotechnical Engineering 110 (8) (1984) 1106–1125.

[33] L. Resende, J. Martin, Formulation of drucker-prager cap model, Journal of Engineering Mechanics 111 (7) (1985) 855–881.

[34] M. Di Croce, F. C. Ponzo, M. Dolce, Design of the Seismic Upgrading of the Tambour of the S. Nicoló's Church in Catania with the DIS-CAM System, in: Structural Analysis of Historic Constructions, Vol. 133 of Advanced Materials Research, Trans Tech Publications, 2010, pp. 947–952.

ACCEPTED MANUSCRIPT

[35] Circ. 2 Feb. 2009 , n. 617, Istruzioni per l'applicazione delle "nuove norme tecniche per le costruzioni" di cui al dm 14/01/2008, Tech. rep., Min. delle Infrastrutture e dei Trasporti (2009).

ACCEPTED MANUSCRIPT